Our responses to the Reviewer are organized as: Reviewer comment in italic and response in blue regular font. The changes made in the manuscript refer to the new version (Page, Line), in bold.

The study of Andersson et al. reports dual isotope analysis method applied to particulate matter in African Savannah region. The study presents little scientific advancement and the value is only related to relatively scarce data from the region impacted by regional biomass burning. However, even that aspect is somewhat compromised due to observational platform located outside biomass burning region to assess full extent of biomass fires. Most of the connecting trajectories do not overpass fire impacted region and not surprisingly reports relatively low concentrations hardly possessing environmental concern. The site is important remote location for climatic observations, but hardly suitable to assess the impact and extent of regional biomass burning. It is, therefore, important to separate samples collected in fire connecting air masses versus unaffected ones to reveal the extent more convincingly. The applied methods are well suited, but their application and especially discussion needs significant improvement. Dual isotope method is well established, but uncertainties related to C13 are downplayed to suit author's narrative. Given combined contribution to C13 ratio from three competing sources (C3, C4 plants and fossil sources) on top of kinetic fractionation affecting the ultimate ratio, uncertainty analysis needs to be much better elaborated and taken into consideration. Monte Carlo simulation is fine, but there is no information on bench-marking – what was the arbiter for the best solution? How Monte Carlo simulation compared to the observed isotope ratios? The paper can be accepted for publication in ACP, but given little scientific advancement requires much more objective consideration of sources, associated uncertainties and Monte Carlo simulation benchmarking.

We thank Reviewer 4 for overall positive assessment for carefully scrutinizing the manuscript and providing valuable suggestions for improvements and clarifications.

We agree with Reviewer (and, in fact, all four reviewers) that the main contributions of the present study lie in the addition to the currently scarce data available for Africa and the isotope-based source constraints. The majority of the overall few ground-based data for Africa are from the western and southern parts, while for central SSA (i.e. Rwanda and neighboring countries) the data is even more scarce. We do emphasize that the present study is the first ever to present ^{14}C-derived source constraints for aerosols at any site in Africa. As such, it is the first to unambiguously differentiate the relative biomass vs fossil fuel contributions with high precision. The strong correlation ($R^2 = 0.85$, $p<0.01$) between the ^{14}C-signature and the inverse of TC concentrations (the Keeling relation) is not only unusual for aerosols - at least we have not found such relations in our previous studies at receptor sites in the Arctic, or South or East Asia (e.g., Winiger et al., 2017; Fang, et al., 2018; Budhavant et al., 2015) - but also provides a clear interpretation: two components explain the source variability at RCO, a background and a seasonally varying biomass source.

The reviewers' comments made us identify three overarching problems with the submitted manuscript. 1.) The representativity of the station w.r.t., air mass transport, 2.) the description of the Monte Carlo techniques and 3.) the statistical treatment of endmember variability, also raised by reviewer 3. We now believe that we comprehensively have addressed these issues, and that the new version of the manuscript is significantly improved.

New/changed figures and tables:

Figure 1: We have updated Figure 1, now with back-trajectory arrival heights at 100 m.a.g.l., and 500 m.a.g.l. as a new Figure S1. In the submitted version the arrival heights were (by mistake) 10 m.a.g.l, and the latitude was slightly offset. We think 100 and 500 are more representative, while they also in good agreement.

Figure 4: We moved the $\Delta^{14}C$ vs TC plot to a new **Figure 5,** in which we also added a $\delta^{13}C$ vs TC plot.

The previous **Figure 5** (2D isotope plot) is the new **Figure 6**.

We have updated the previous **Figure 6** with the results from the new MCMC approach, and this is the new **Figure 7**.

New Figure S1: back trajectories at arrival height 500 m.a.g.l.

New Figure S2: $\Delta^{14}C$ vs TC and $\delta^{13}C$ vs TC from the new Bayesian MCMC source apportionment method,

New Figure S3: A sensitivity analysis of the new Bayesian MCMC source apportionment strategy w.r.t. number of data points.

New Figures S4-S6: computed fractional source contributions from 3 alternative endmember scenarios; sensitivity tests.

New Table S2 with updated fractional source contributions from the new MCMC approach.

New Tables, S3-S5: results from the MCMC-based source apportionment from the 3 alternative endmember scenarios.

We detail our responses and actions to these main comments below, while responses to the specific comments comes after.

1.) Back-trajectories:

We thank the Reviewer to highlighting concerns regarding the back-trajectories. This made us go back and re-evaluate them. The arrival height, 1600 m.a.s.l., used in the manuscript is 10 m.a.g.l. However, this height is low, and our original intention was to use 100 m.a.g.l.; the discrepancy is explained by an erroneous input of the height of Mt. Mugogo, 1500 compared to the actual 1590. To resolve this issue, we have now re-computed the back-trajectories for two arrival heights: 100 m.a.g.l. (1690 m.a.s.l.) and 500 m.a.g.l. (3090 m.a.g.l), see below response figures R1 and R2:

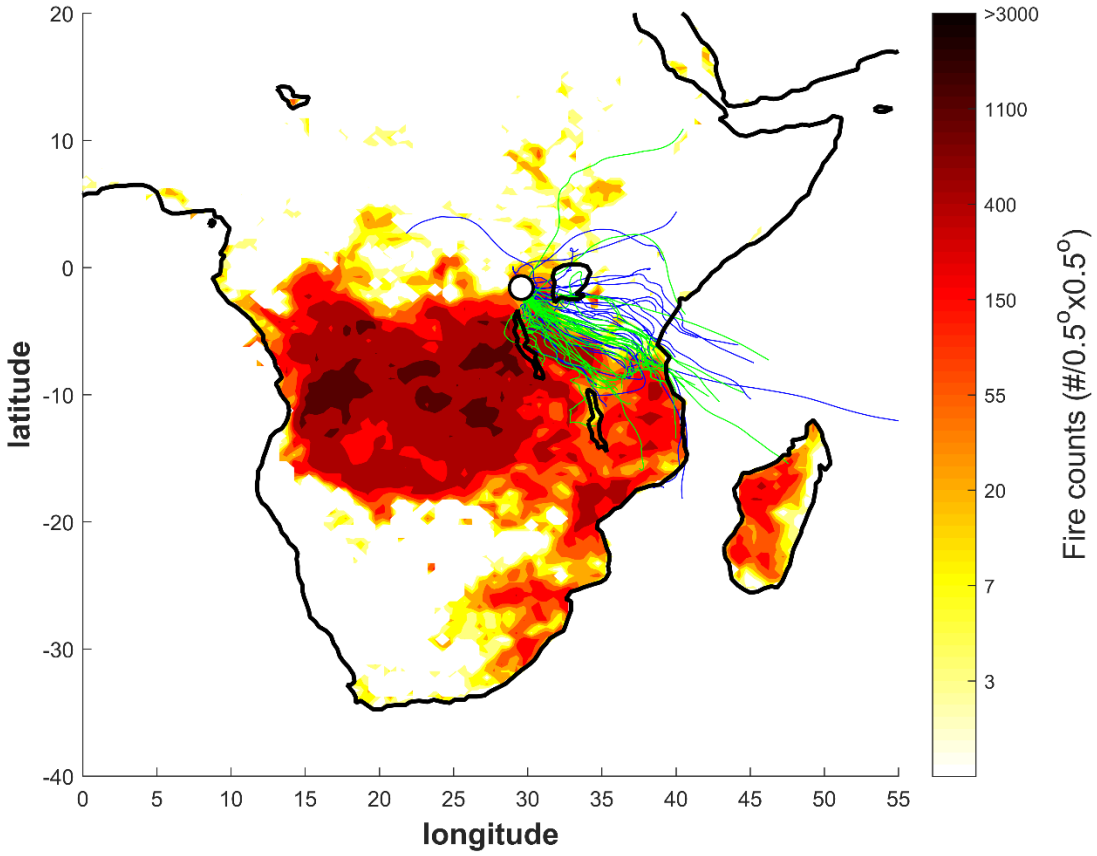

Figure R1 Fire counts and air mass back trajectories for the October 2014 to September 2015 campaign at the Rwanda Climate Observatory (RCO, black and white circle). The fire counts arefrom the Fire Information for Resource Management System (FIRMS) derived from the NASA 659 Moderate Resolution Imaging Spectroradiometer (MODIS) satellite product for June-July-August (JJA), 2015. The thin lines represent daily (4AM, C.A.T.) 5-day air mass back-trajectories arriving at RCO 100 m.a.g.l. (2690 m.a.s.l.). The blue lines correspond to what we here refer to the 'wet' period (October-November 2014 and April-May 2015), whereas the green lines represent the dry JJA period.

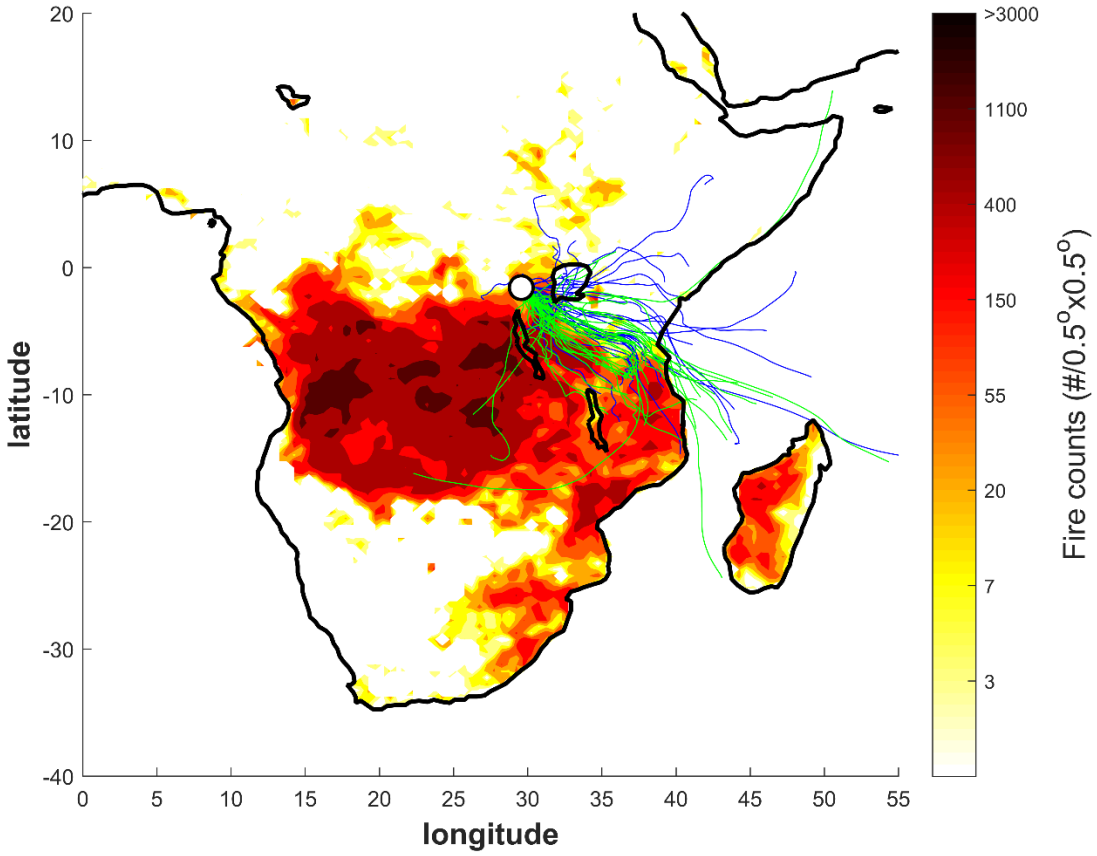

Figure R2 Fire counts and air mass back trajectories for the October 2014 to September 2015 campaign at the Rwanda Climate Observatory (RCO, black and white circle). The fire counts arefrom the Fire Information for Resource Management System (FIRMS) derived from the NASA 659 Moderate Resolution Imaging Spectroradiometer (MODIS) satellite product for June-July-August (JJA), 2015. The thin lines represent daily (4AM, C.A.T.) 5-day air mass back-trajectories arriving at RCO 500 m.a.g.l. (3090 m.a.s.l.). The blue lines correspond to what we here refer to the 'wet' period (October-November 2014 and April-May 2015), whereas the green lines represent the dry JJA period.

Taken together, we find that the reviewer's comment on the representativity of RCO for capturing biomass burning episodes in Southern Africa now should be resolved. The dry period BTs are clearly overlapping with FIRMS fire spots. We furthermore note good agreement between the BTs at the two arrival heights at 100 and 500 m.a.g.l., adding to our confidence of air mass history representativeness. These air mass transport pathways are also in better agreement with the description for RCO provided in DeWitt et al. (2019). Finally, we note that it is re-assuring that the source characteristics present in our chemical and isotope data now are in better agreement with air mass history.

We have now replaced the old Figure 1 with the new plot with 100m arrival heights (R1), and the 500m arrival height figure (R2) is the new Figure S1 in the SI.

2.) Monte Carlo Simulations

We agree that the details regarding the MCMC methods should be more comprehensive. We address the topics of convergence and general description, and comparison of observational isotope signatures and back-calculated values here. This discussion is further elaborated upon in the section 3.) on endmember variability.

MCMC Convergence

The Monte Carlo-based technique used here is based on our method described in detail in Andersson et al. (2015). Based on a Bayesian statistical problem formulation, this method will provide robust source quantification and uncertainty estimation, given the underlying probabilistic assumptions and endmember distributions. However, we agree that we have omitted important details regarding the details on this method. As described below, we have now chosen to implement a slightly more advanced source apportionment model, but the generic MCMC parameters remain the same. See added text below.

'The source fractions were computed using numerical Markov chain Monte Carlo simulations, implemented in Matlab, ver. 2015b, using 1000.000 iterations with a burn-in (initial search phase) of 10.000 and a data thinning of 10 (removing step-wise correlations). The stochastic perturbation parameter was adjusted as to obtain an acceptance ratio of 0.23, which has been suggested to be optimal for Metropolis-Hastings algorithms (Roberts et al., 1997). For this set-up, the variability in the numerically estimated parameters, e.g., the standard deviation of the relative source fraction, is lower than 1% of the mean value, suggesting good convergence (Winiger et al., 2017)'

Line 9 Lines 207-213

Mass balance-based source apportionment

Overall, we think the back-calculation of observed isotope signatures from the estimated source fractions is an interesting point. However, since mass-balance source apportionment is an inverse technique, error propagation is inherently non-linear, e.g., new version of Eq. (1):

$$f_{bio} = \frac{\Delta^{14}C_{sample} - \Delta^{14}C_{fossil}}{\Delta^{14}C_{bio} - \Delta^{14}C_{fossil}}$$

Furthermore, since we compute source fractions there is a correlation between the central value the variability. Taken together, isotope-values back-calculated from the estimated fraction is theoretically not expected to agree when the variability is large (see, e.g., Andersson, 2012). In fact, the estimated source fractions will tend to equal proportions as a function of increasing endmember variability; the sources become indistinguishable in the limit of very large uncertainties.

After careful consideration of the Reviewer comments regarding endmember uncertainties we have decided to implement a more in-depth Bayesian isotope mass-balance model Martens et al., 2019), described below.

The comparisons between observational and back-calculated isotope ratios are therefore presented in this context, Figs. R5 and R6.

Figures R5 and R6 combine to a new SI figure 2. And a corresponding comment in the main manuscript:

'Back-calculating the isotope signatures from the computed source fractions from the MCMC-simulations essentially reproduce the Keeling relations relative to 1/TC (Figs. 5 and S2).'

Page 15 Lines 388-390

3.) Endmember variability

An alternative source apportionment model

The isotope endmembers used in the present study are what is essentially measured at 'the tailpipe' of an emission source, and is strongly affected by, e.g., combustion efficiency and the isotope signature of the fuels. This introduce a large variability in the data. However, this large variability is not expected in the atmosphere, where mixing will average the signal from a given source type, e.g., a savanna fire, or source fuel, e.g., C_4-plants, and the values will tend to the mean, including kinetic isotope effects (KIE). Thus, source apportionment should therefore ideally be conducted using such averaged signals. However, we do not have this type of data, and estimating the degree of averaging is not straight-forward a priori. If, on the other hand, one can use correlations between the data points, a means for constraining the effective endmember variability at the measurement site can be obtained. Such correlations may be w.r.t. time, concentrations or other parameters.

In the present study, we find that the $\Delta^{14}C$ is well correlated ($R^2 = 0.85$, $p<0.01$) with 1/TC - the 'Keeling relation', Fig. R3 (original Figure 4C), while the correlation of $\delta^{13}C$ vs 1/TC is weaker ($R^2 = 0.56$, $p<0.1$), Fig. R4. The correlation with $\Delta^{14}C$ is unambiguous in the sense that $\Delta^{14}C$ is not affected by kinetic isotope effects, and the endmember values are well-constrained: it directly reports on the relative contributions of biomass/biogenic vs fossil contributions. We thus know that the source-relation exhibited in the $\Delta^{14}C$ data is also present in the $\delta^{13}C$ data, but the weaker $\delta^{13}C$ vs 1/TC trend is due larger endmember variability, and potential kinetic isotope effects. These relations can be used a means for including data correlations in Bayesian MCMC-based source apportionment; accounting for the effects of endmember averaging during air mass transport. Indeed, we have developed such method, with the theoretical basis presented in detail in Martens et al. (2019). This model is essentially an extension of the method used in the original submission: the endmember representation remains the same, but we add the correlations with 1/TC. We emphasize that since the $\Delta^{14}C$ vs 1/TC correlation is stronger, this will impose stronger source constraints than the $\delta^{13}C$ vs 1/TC relation; the strength of the correlation is naturally incorporated within this framework, e.g., compare Figures R3 and R4 with the corresponding Figure R6 and R7.

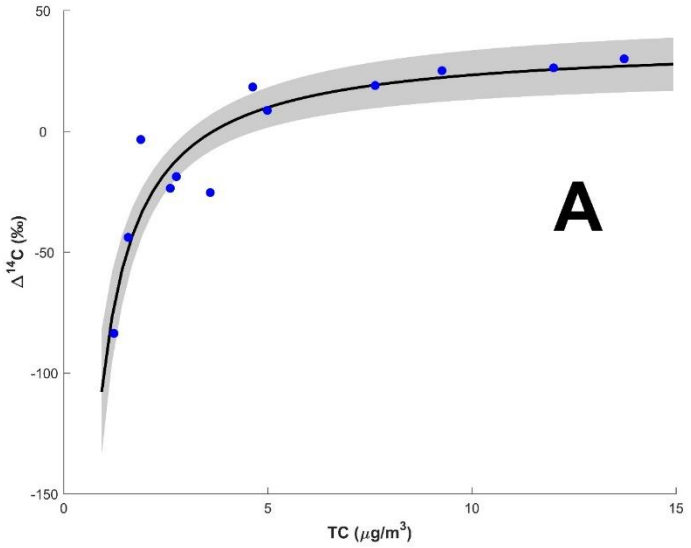

Figure R3 MCMC fit of $\Delta^{14}C$ vs TC.

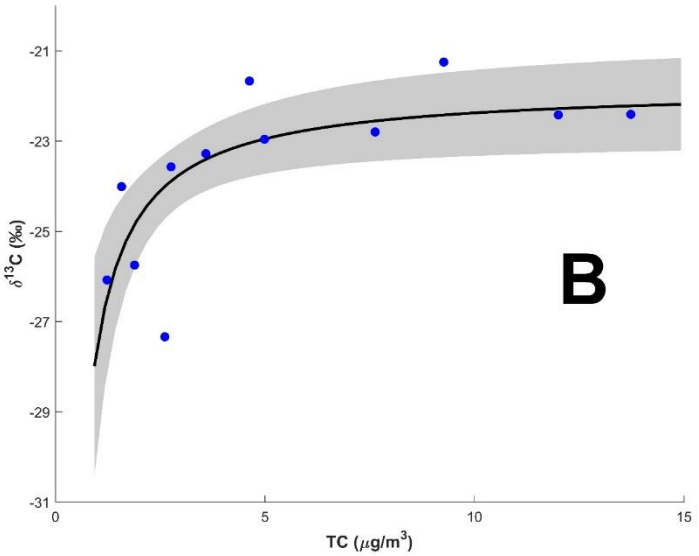

Figure R4 MCMC fit of $\delta^{13}C$ vs TC.

Figures R3 and R4 are now Panels A and B in the new Figure 4 in the revised manuscript.

The statistical strength of the method of Martens et al. compared to the method used in the original submission is illustrated by the number of fitting parameters used in the analysis. In the original submission (where no correlations between data points are used) we fit 24 independent parameters (noting that $f_{C3} + f_{fossil} + f_{C4} = 1$; two independent variables) to 24 data points (12 $\Delta^{14}C$ and 12 $\delta^{13}C$). In the 'Keeling method' we fit 4 independent parameters (2 for the slope and 2 for the intercept of the line) to 24 data points.

In addition, we have conducted a sensitivity analysis of the new source apportionment approach w.r.t. the number of data points included in the calculated. To compare with the scenario where all data points are used, we computed scenarios where only every third point is used (3 scenarios, starting at data point 1, 2 and 3, respectively). We find that the number of data points has a strong influence (as expected) on the computed results, and that the uncertainties on average double in the 'every-third' scenarios. We have added a new Figure S3 (R5), displaying the comparison, and the following text in the R&D:

'To check influence of the number of data points used in the Keeling-based MCMC, we computed comparative scenarios where every third data point was used (starting at data point 1, 2 and 3 respectively) (Fig S3). The standard deviations for the calculated f_{C3} are on average doubled when only every third point are used (5% vs 10%), showing how correlations between multiple data points aids in constraining the sources'

Page 15 Lines 390-394

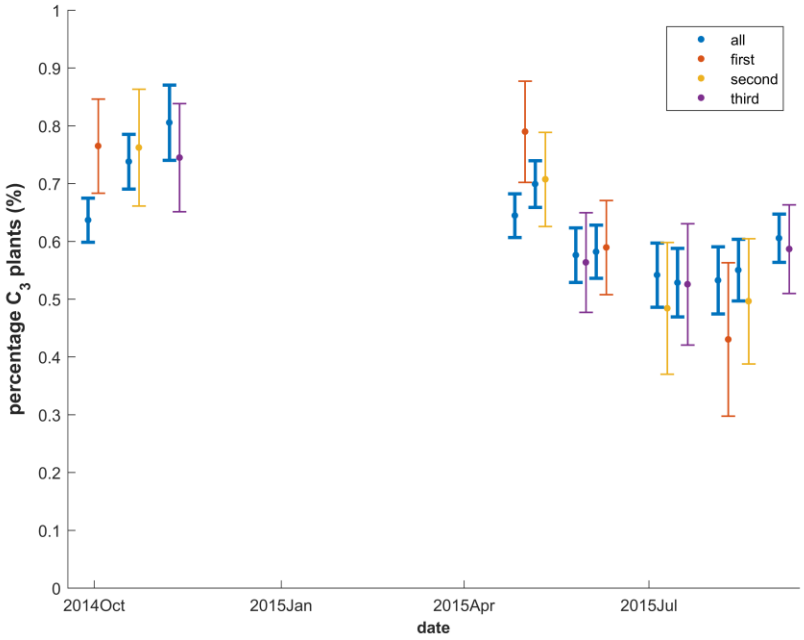

Figure R5 Sensitivity of the Keeling-based Bayesian MCMC source apportionment approach w.r.t. number of data points in the calculation. The fraction C_3-plants is plotted vs time. In blue, the results from using all 12 data pairs (errorbars: mean ± stdev). The orange, yellow and purple lines show calculations using every third data point, starting from data point 1, 2 and 3, respectively. The results from every third data points are shifted slightly in time (to the right) for visual clarity.

As we believe that this method is more statistically and physically sound for the present analysis, we implement this approach. For discussion of the results of this methodology, see below discussion on endmember sensitivity analysis.

We have replaced the old model description in the M&M section with:

'The vegetation in SSA may be divided into two main photosynthetic classes: C_3-plants and C_4-plants, see discussion in Section 3.5. These two groups have distinct $\delta^{13}C$-signatures, allowing isotope-based separation. We may then resolve three source classes by combining $\Delta^{14}C$ and $\delta^{13}C$: C_3-plants, C_4- plants and fossil, through isotopic mass-balance (Andersson et al., 2015):

$$\begin{pmatrix} \Delta^{14}C(i) \\ \delta^{13}C(i) \\ 1 \end{pmatrix} = \begin{pmatrix} \Delta^{14}C_{C3} & \Delta^{14}C_{fossil} & \Delta^{14}C_{C4} \\ \delta^{13}C_{C3} & \delta^{13}C_{fossil} & \delta^{13}C_{C4} \\ 1 & 1 & 1 \end{pmatrix} \begin{pmatrix} f_{C3}(i) \\ f_{fossil}(i) \\ f_{C4}(i) \end{pmatrix} \quad (2)$$

Endmember variability may significantly influence the calculated source fractional contributions (Andersson, 2011). For a discussion on the specific endmember ranges used here, see Section 3.5.

In Eq. (2) the isotopic data is treated as independent. However, here we find that there is a dependence between the isotope ratios and the TC concentrations, such that $\Delta^{14}C(i) \sim A/TC(i) + B$, where A and B are constants, and i is the sample index (Fig. 5). This is known as a Keeling relation, and is discussed in more detail in Section 3.4. The relation holds for both $\Delta^{14}C$ (R^2=0.85, $p<0.01$) and $\delta^{13}C$, while the correlation is weaker for $\delta^{13}C$ (R^2=0.55, $p<0.1$). A method for using correlations within the framework Bayesian source apportionment has recently been developed (Martens et al., 2019). The rationale is based on both statistical concepts and the averaging expected from atmospheric mixing. The endmember ranges used in the calculations are from isolated sources, but during long-range transport the variability within a given source, e.g., savanna fires, will be reduced. Using correlations between data points, a means for accounting for the mixing is obtained, and more realistic source fraction estimates are obtained. When using the estimated source fractions to back-calculate the isotope signatures, the agreement is good compared with direct fits (Fig. 5 and Fig. S2). A sensitivity analysis is discussed in section 3.5 (Fig. S3)

To account for the correlations in the data-set we therefore add a second constraint in the source apportionment calculations, based on the relation to the TC concentrations:

$$\begin{pmatrix} f_{C3}(i) \\ f_{fossil}(i) \\ f_{C4}(i) \end{pmatrix} = \frac{1}{[TC(i)]} \cdot \begin{pmatrix} f_{C3,slope} \\ f_{fossil,slope} \\ f_{C4,slope} \end{pmatrix} + \begin{pmatrix} f_{C3,intercept} \\ f_{fossil,intercept} \\ f_{C4,intercept} \end{pmatrix} \quad (3)$$

Where we, instead of fitting a source vector (f_{C3}, f_{fossil}, f_{C4}) for each individual data pair, fit two vectors: a slope and an intercept of the line, to all data points. This clearly holds the advantage of have fewer fitting parameters. We emphasize that the strength of the correlation of the isotope signatures relative to 1/TC is naturally incorporated into this relation, such that lower correlation of $\delta^{13}C$ w.r.t 1/TC impose weaker constraints on the calculated source fractions, compared to $\Delta^{14}C$.'

Pages 7-9 Lines 178-206

Observational vs estimated isotope signatures

To address the Reviewers' comment on comparing the original isotope data with back-calculated parameters, we here present these using the newly implemented Bayesian MCMC model plotted w.r.t. the TC concentrations, Figures R5 and R6. In we see that the estimated $\delta^{13}C$ parameters from the MCMC-based source apportionment strategy essentially replicates Figure R3 and R4, suggesting good agreement, despite the non-linearity of inversion, discussed above.

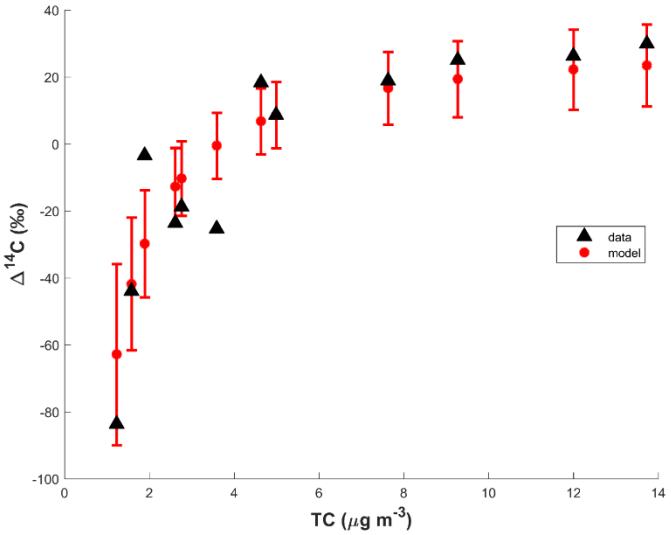

Figure R6 Comparison of observed carbon isotope signatures (black triangles) for TC and values back-calculated from the MCMC-estimated source fractions using the 'best endmember scenario' (red circles with errorbars). Panel A. $\Delta^{14}C$ vs TC. Panel B. $\delta^{13}C$ vs TC.

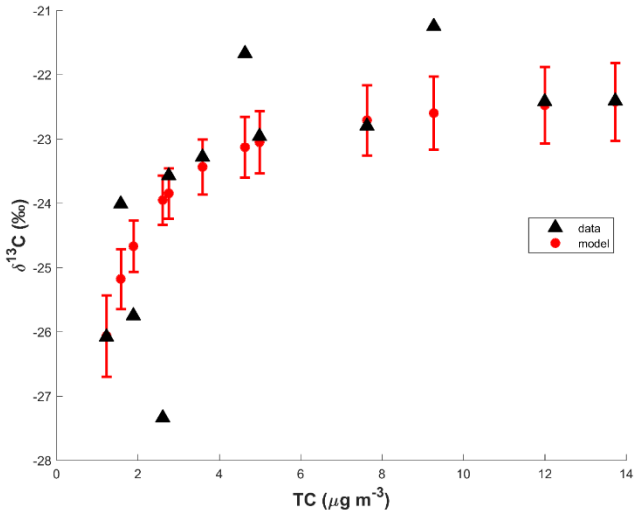

Figure R7. Comparison of observed carbon isotope signatures (black triangles) for TC and values back-calculated from the MCMC-estimated source fractions using the 'best endmember scenario' (red circles with errorbars). Panel A. $\Delta^{14}C$ vs TC. Panel B. $\delta^{13}C$ vs TC.

Figures R6 and R7 combine to a new Figure S2, and we have added the following text to the main manuscript:

'When using the estimated source fractions to back-calculate the isotope signatures, the agreement is good compared with direct fits (Fig. 5 and Fig. S2).'

Page 8, Lines 195-197

Endmember sensitivity tests

The reviewer raises concerns w.r.t. endmember variability and representativity. Here we address four different endmember scenarios, see also responses to specific points below:

a. *The 'original' best scenario:*
   $\delta^{13}C_{C3}$ = -27.1 ± 2.2 ‰; $\delta^{13}C_{fossil}$ = -25.5 ± 1.3 ‰; $\delta^{13}C_{C4}$ = -16.6 ± 2.2 ‰
b. *The 'no-KIE C_4' scenario:*
   $\delta^{13}C_{C3}$ = -27.1 ± 2.2 ‰; $\delta^{13}C_{fossil}$ = -25.5 ± 1.3 ‰; $\delta^{13}C_{C4}$ = -13.1 ± 1.2 ‰
   Where the $\delta^{13}C$ endmember range of C_4 is not affected by any KIE depletion.
c. *The 'max-KIE C_4' scenario:*
   $\delta^{13}C_{C3}$ = -27.1 ± 2.2 ‰; $\delta^{13}C_{fossil}$ = -25.5 ± 1.3 ‰; $\delta^{13}C_{C4}$ = -19.0 ± 2.2 ‰
   This scenario corresponds to the point where the estimated $f_{C4}/(f_{C4} + f_{C3})$ = 0.64 in the limit TC $\rightarrow\infty$; the signature expected from pure savanna fires.
d. *The 'depleted fossil' scenario:*
   $\delta^{13}C_{C3}$ = -27.1 ± 2.2 ‰; $\delta^{13}C_{fossil}$ = -28.5 ± 1.3 ‰; $\delta^{13}C_{C4}$ = -16.6 ± 2.2 ‰
   In this scenario we shifted the fossil average by -3 ‰. There is no real quantitative argument for this depletion, other than it represents a large shift.

a. The original scenario

In this scenario we use the endmember ranges presented in the original submission, but with the source apportionment strategy from Martens et al. (2019), Fig. R8 is the new Figure 7. Compared to the original submission, we find that this method provides a significantly larger separation between the relative C_3 and C_4 plant contributions, with a suppression of the estimated uncertainties, see also above discussion regarding a sensitivity of the new MCMC strategy w.r.t. number of data points.

In the limit of TC approaching infinity, $f_{C4}/(f_{C4} + f_{C3})$ = 0.47 for this scenario. Since the $f_{C4}/(f_{C4} + f_{C3})$-value for East African savannas is ~ 0.64, this limit would correspond to 74% savanna contributions.

This scenario is what we consider to be the most likely, as it is represents the average of the no KIE scenario and the maximum KIE-induced ^{13}C depletion observed (-7‰).

New text in the main manuscript:

‘Accounting for such effects in source apportionment is a challenge, especially since the reported values are ranges and not mean and variability, and thus are highly influenced by potential outliers. We here use a method discussed in Andersson et al. (2015) to address the issue of statistical analysis of ranges by assuming that the total range corresponds to the 95% confidence intervals of a normal distribution. This corresponds to the range of 4 times the standard deviation, yielding σ = 7/4‰, while the mean is -7/2‰. Combining this with the variability of the of pure C_4-plants we obtain: $\delta^{13}C_{C4}$: -16.6 ± 2.2‰, where $\sigma^2 = 1.2^2 + (7/4)^2$ ‰^{2}. These values are also what is obtained by numerical estimation of the convolution of a normal distribution (μ = -16.6, σ = 1.2‰) with a uniform distribution ([-7, 0] ‰), adding to the strength of statistical representation.’

Page 14-15 Lines 369-377

Table S2 is updated accordingly.

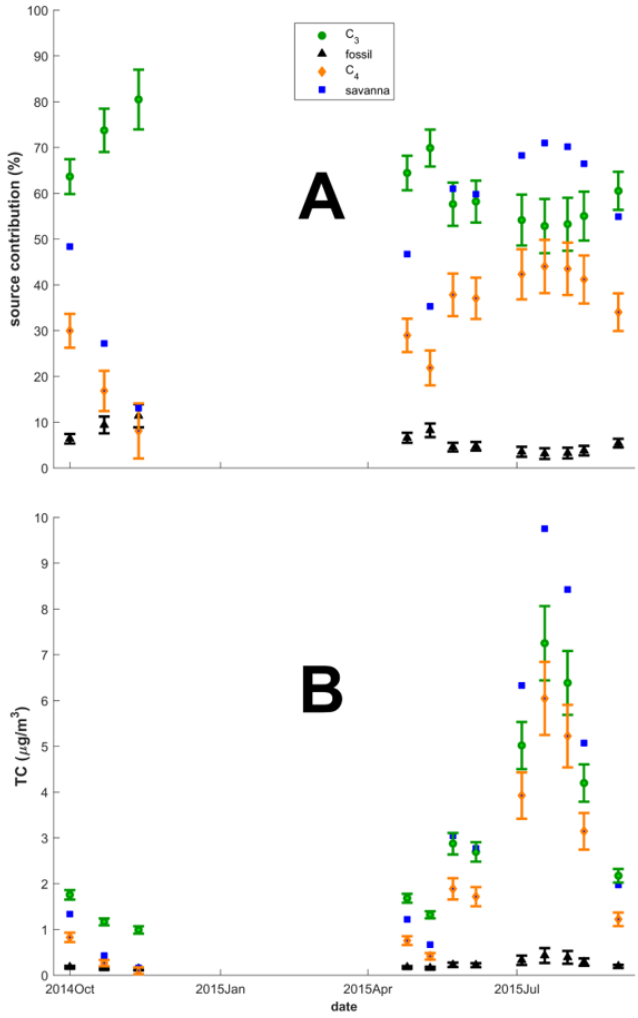

Figure R8 Estimated source fractions and source-segregated TC concentrations with the **original endmember scenario.**

b. The no KIE scenario

This scenario corresponds to the case where the $\delta^{13}C_{C4}$ of aerosols is not associated by any ^{13}C-depletation by KIE. Consequently, it is a 'minimum C_4' scenario. In the limit of TC approaching infinity, $f_{C4}/(f_{C4} + f_{C3})$ = 0.36 corresponding to 55% savanna. This is thus the lower bound for savanna contributions int the TC→∞ limit, as is apparent in Fig R9. However, it is not a likely scenario, as there are known KIEs in aerosols emitted from C_4 incomplete combustion.

Figure R9 is a new Figure S5, and the results are added in the new Table S4.

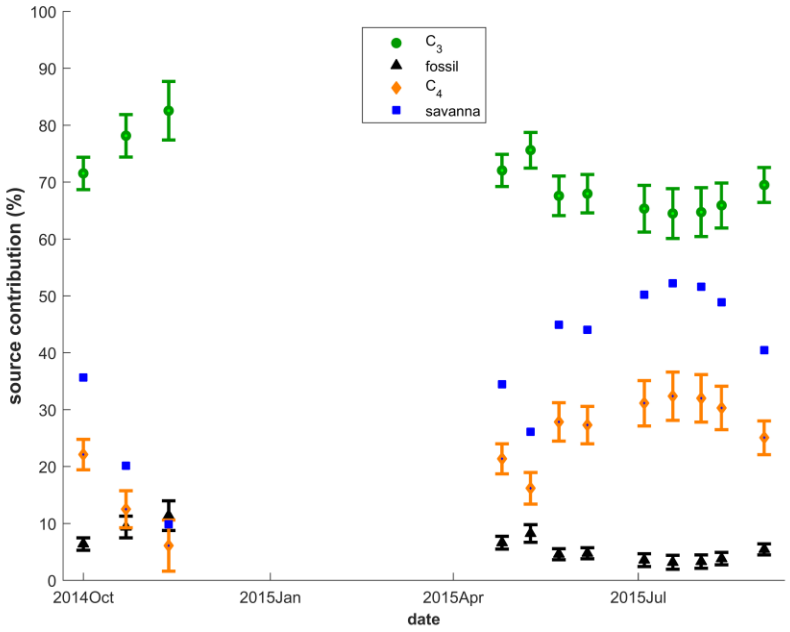

Figure R9 Estimated source fractions with the **no-KIE endmember scenario.**

c. The max-KIE scenario

In this scenario we use the $\delta^{13}C_{C4}$ endmember values that corresponds to the $f_{C4}/(f_{C4} + f_{C3})$ observed in East African savannas, 0.62, Fig. R9. The KIE is -5.9‰ relative to pure C_4-plants, and we thus would have 100% savanna fire contributions in the TC→∞ limit. As for point c, this is an extreme limit scenario and is less likely than the original 'best' scenario.

Figure R10 is a new Figure S4, and the results are added in the new Table S3.

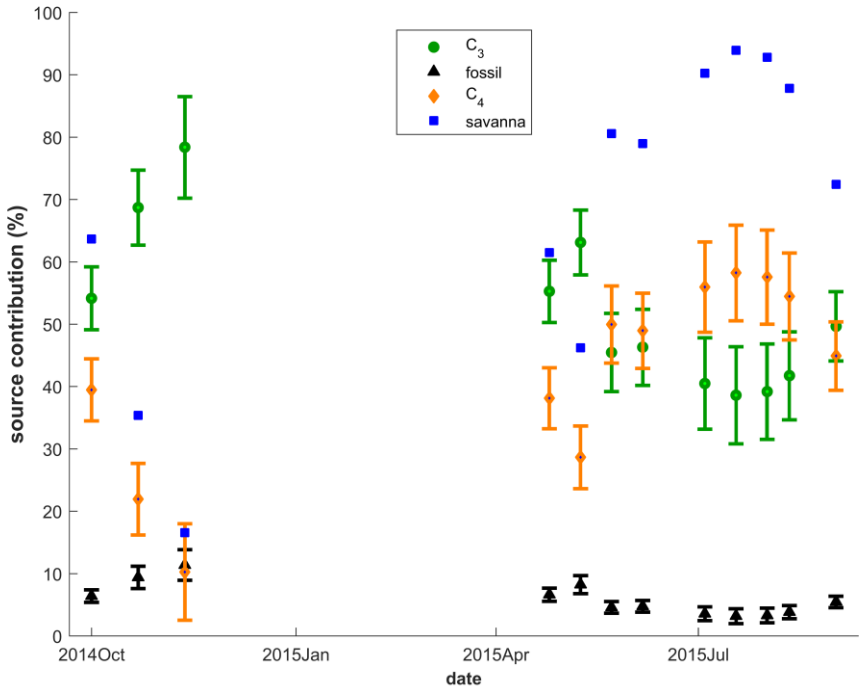

Figure R10 Estimated source fractions with the **max-KIE endmember scenario**.

d. The depleted fossil scenario

In this scenario we shift the fossil $\delta^{13}C$ endmember by -3‰, Fig. R11. In this scenario the fossil fractions shift by less than 5%. This is not surprising, as the main determinant of the fossil contributions is the $\Delta^{14}C$ data Given the low overall fossil contributions (15%<), this shift in $\delta^{13}C_{fossil}$ does not propagate into the differentiation between C_3 and C_4 plants. Overall, we conclude that the set-up is not sensitive to the fossil $\delta^{13}C$ endmember for the present data.

Figure R11 is a new Figure S6, and the results are added in the new Table S5.

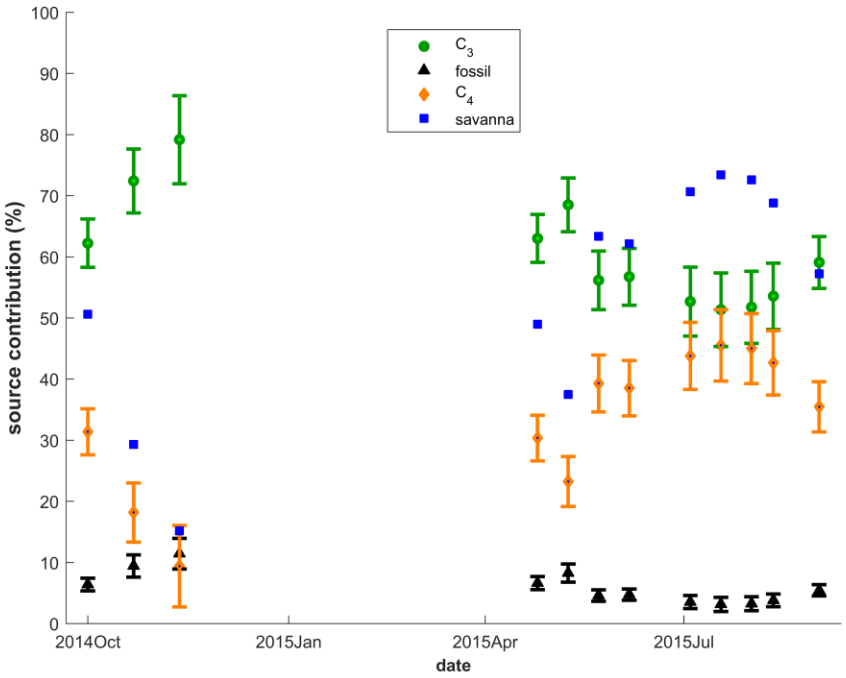

Figure R11 Estimated source fractions with the **depleted fossil endmember scenario**.

Overall, we conclude that:

1. That, as expected, the value of the C_4 $\delta^{13}C$ influence the estimated fractional C_4 contributions, such that the larger the KIE the larger the fraction C_4.
2. The estimated source fractions are insensitive to the $\delta^{13}C$-fossil endmember.
3. The sensitivity analysis from the maximum and minimum KIE C_4 $\delta^{13}C$ endmember shows that the savanna contributions may span 55% to 100%. However, the original best scenario is the most un-biased representation.

We have added the following text to the R&D:

'Since the $\delta^{13}C$ endmembers for, in particularly C_4-plants, are not well-constrained, we also employed a sensitivity analysis w.r.t. endmembers and the potential influence of KIE (Tables S2 – S5 and Figs. S4 – S6). In addition to the above discussed best estimate scenario, we tested two $\delta^{13}C_{C4}$ scenarios: a 'minimum KIE scenario' with zero KIE ($\delta^{13}C_{C4}$ -13.1±1.2‰) and a 'maximum KIE scenario', with a depletion by 5.9‰ ($\delta^{13}C_{C4}$ -19.0±2.2‰). The maximum KIE scenario was established such as the $f_{C4}/(f_{C4}+f_{C3})$-ratio would be 62% as TC approach infinity, and thus 100% savanna contributions, see Eq. (4). As expected, these scenarios significantly shift the estimated relative C_4 contributions, resulting in a total range of the sample period averages of 24% (min-KIE; min 6% max 32%) to 42% (max-KIE; min 10%, max 58%), thus providing lower and upper bounds (Figs. S4 and S5 and Tables S3 and S4). The corresponding value for

our best estimate is 32% (max 44%, min 8%). In addition, we investigated a scenario with a 3‰ depletion of the fossil endmember ($\delta^{13}C_{fossil}$ -28.5±1.3‰). Since the fossil contribution is overall low as determined by $\Delta^{14}C$, and since $\Delta^{14}C$ constrains the fossil contribution independently of the $\delta^{13}C$ data, this shift has no significant influence on the computed source fractions 6% (max 11%, min 3%) (Fig. S6 and Table S5). Overall, we stress that these three sensitivity test scenarios represent extreme limits, and the a priori least biased scenario is the initially outlined best scenario.'

Pages 15-16 Lines 395-410

4. Responses to specific comments

Line 235. Out-gassing SO2 emissions can contribute very significantly to regional sulphate levels even without recognised volcanic activity (Ovadnevaite et al. 2009).

We agree. We now write.

'RCO is situated not far away from the Nyiargongo and Nyamuragria Volcanoes in eastern Democratic Republic of Congo. High spatial resolution (13x24km^2) satellite-monitoring of the SO_2 levels show a near-constant emissions from these volcanoes over the time period covering the present campaign, likely affecting the observed sulfate levels (Barrière et al., 2017). Here we observe a spike in sulfate levels (~ 5µg m^{-3}) during the week starting of the 13th of June 2015 (Fig. 2), but with no clear linkage to an increase in volcanic SO_2 emissions'

Page 11 Lines 259-264

Line 246. Authors may also consider that OC/EC ratio is very dependent on the combustion stage - flame fires versus smouldering fires.

This is certainly true. We now emphasize this fact:

'The OC/EC-ratio is sometimes used as a marker for biomass burning, but is highly influenced by burning conditions such as flaming or smoldering fires.'

Page 11 Lines 271-272

Line 321. d13 fossil ratio is very much region dependent and needs to be better constrained or uncertainty increased. It is possible that African liquid fossil fuel isotopic signatures are around -25, but it can be as low as -29 in other regions and, therefore, should be much better constrained or proven or uncertainty increased.

We agree that there can be high regional variability, emphasizing the crucial need to incorporate endmember variability in source apportionment calculations. In earlier publications, we have recognized

that the $\delta^{13}C$ for Russian liquid fossil fuels, is more in the range of -31 per mille, while the majority of other fuels are in the presently used range (Winiger et al., 2017). In the above sensitivity test we show that the exact value of the fossil endmember has little influence on the presently evaluated source fractions, Fig R10.

See above revisions in the new manuscript.

Line 328. Why the uncertainty of of C4 isotopic signature is twice smaller than of C3 plants? It also contradicts Figure 5 where C4 signature is ~16.5+/-2. That seems to be biased low as C4 signatures are more in the region of -16 to -10 (something like -13+-3). C4 signatures need to be much better constrained which will have significant impact on source contribution and associated uncertainty.

A priori, there is no clear reason as to why the variability of either C_3 or C_4 should be smaller, larger or similar. However, one may use evolutionary/ecological arguments to explain why the variability of C_4 might be expected to be smaller: C_4-plants branched off from the C_3-plants stem in the evolutionary tree to colonize a comparably specific ecological niche: hot and dry conditions (e.g., savannas). C_3-plants, on the other hand, are abundantly present in a much wider array of ecological niches, including savannas, boreal forests, marine environements etc. Adaption to a wide array of environmental conditions is expected to affect the $\delta^{13}C$, either evolutionary (genetically) or physiologically, such that the variability will increase.

No citation is provided for the number -13+-3. Here, we have cited extensive reviews (based on 'hundreds of papers') on the subject of the $\delta^{13}C$-values of C_4-plants, arriving at the value used here (Bender et al., 1971; O'Leary et al., 1988; Turekian, 1998). However, the main uncertainty here lies not in the $\delta^{13}C$-values themselves, but in the kinetic isotope effects associated with combustion and transformation into aerosols. Here, the literature is scarce, and mainly provide ranges, which are hard to evaluate statistically, as they may be very biased towards outliers. **See above changes in the manuscript**

Line 342. The result is highly contentious. Why only C4 plants burning are dominant during dry season? While only C3 plants contribute to wet season SOA? The statement contradicts Figure 6 where C4 and C3 contribution is about equal even during dry season.

We have significantly changed this section, see above responses.

Figure 6 does not fit discussion and seem to be interpreted very subjectively.

See above discussion

Outlook section The authors should not discuss implications beyond presented data. Cloud brightening and broad climatic implications are not supported by the study data and seem to be out of place.

We agree to some extent, and have reduced the Outlook section, and removed, e.g., the discussion on cloud brightening. However, we do maintain that a broader discussion on implications is warranted in an outlook section (it is not a summary or conclusions part).

Figure 4. Uncertainty error bars are absent in the Figure.

The uncertainties for $\Delta^{14}C$ are below 50‰ and ~ 0.2‰ for $\delta^{13}C$. We have added this information to the figure legend for visual clarity.

References

Andersson, A.: A systematic examination of a random sampling strategy for source apportionment calculations. Sci. Tot. Environ. 412-413, 232-238, doi: 10.1016/j.scitotenv.2011.031, 2011.

Andersson, A., Deng, J., Du, K., Zheng, M., Yan, C., Sköld, M., Gustafsson, Ö.: Regionally-varying combustion sources of the January 2013 severe haze events over Eastern China. Environ. Sci. Technol. 49, 2038-2043, doi: 10.1021/es503855e, 2015.

Bender, M.M.: Variations in the $^{13}C/^{12}C$ ratios of plants in relation to the pathway of photosynthetic carbon dioxide fixation. Phytochem. 10, 1239-1244, doi: 10.1016.S0031-9422(00)84324-1, 1971.

Budhavant, K., Andersson, A., Bosch, C., Kruså, M., Kirillova, E.N., Sheesley, R.J., Safai., P.D., Rao, P.S.P., Gustafsson, Ö.: (2015) Radiocarbon-based source apportionment of elemental carbon aerosols at two South Asian receptor observatories over a full annual cycle. Environ. Res. Lett. 10, doi: 10.1088/1748-9326/10/6/064004.

Fang, W., Du, K., Andersson, A., Zing, Z., Cho, C., Kim, SW., Deng, J., Gustafsson, Ö.: (2018) Dual-Isotope Constraints on Seasonally Resolved Source Fingerprinting of Black Carbon Aerosols in Sites of the Four Emission Hot Spot Regions of China. J. Geophys. Res. doi: 10.1029/2018JD028607.

Martens, J., Wild, B., Pearce, C., Tesi. T., Andersson, A., Bröder, L., O'Regan, M., Jakonsson, M., Sköld, M., Gemery, L., Cronin, T.M., Semiletov, I., Dudarev, O.V., Gustafsson, Ö.: (2019) Remobilization of Old Permafrost Carbon to Chukchi Sea Sediments During the End of the Last Deglaciation. Glob. Biogeochem. Cyc. 33, 2-14, doi: 10.1029/2018GB005969.

O'Leary, M.H.: Carbon isotopes in photosynthesis. Bioscience 38, 328–36, doi: 10.2307/1310735, 1988.

Roberts, G.O., Gelman, A., Gilks, W.R.: (1997) Weak convergence and optimal scaling of random walk Metropolis algorithms. Ann. Appl. Prob. 7, 110-120.

Turekian, V. C., Macko, S., Swap, R. J. and Garstang, M.: Causes of bulk carbon and nitrogen isotopic fractionations in the products of vegetation burns: laboratory studies. Chem. Geol. 152, 181-192, 10.1016/S0009-2541(98)00105-3, 1998.

Winiger, P., Andersson, A., Eckhardt, S., Stohl, A., Semiletov, I.P., Dudarev, O.V., Charkin, A., Shakova, N., Klimont, Z., Heyes, C., Gustafsson, Ö.: (2017) Siberian Arctic black carbon sources constrained by model and observation. Proc. Nat. Acad. Sci. doi: 10.1073/pnas.1613401114.

Winiger, P., Barrett, T.E., Sheesley, R.J:, Huang, L., Sharma, S., Barrie, L.A., Yttri, K.E., Evangeliou, N., Eckhardt, S., Stohl, A., Klimont, Z., Heyes, C., Semiletov, I.P., Dudarev, O.V., Charkin, A., Shakhova, N., Holmstrand, H., Andersson, A., Gustafsson, Ö.: Source apportionment of circum-Arctic atmospheric black carbon from isotopes and modelling. Sci. Adv. 5, doi: 10.1126/sciadv.aau8052, 2019.